

**“Biogas valorization via continuous polyhydroxybutyrate production
by *Methylocystis hirsuta* in a bubble column bioreactor”**

**Yadira Rodríguez^{a,b}, Paulo Igor Milen Firmino^{b,c}, Víctor Pérez^{a,b}, Raquel
Lebrero^{a,b}, Raúl Muñoz^{a,b,*}**

^a Department of Chemical Engineering and Environmental Technology, School of Industrial
Engineering, University of Valladolid, Dr. Mergelina s/n, 47011 Valladolid, Spain

^b Institute of Sustainable Processes, Dr. Mergelina s/n, 47011 Valladolid, Spain.

^c Department of Hydraulic and Environmental Engineering, Federal University of Ceará,
Fortaleza, Ceará, Brazil

* Corresponding author: mutora@iq.uva.es

1 **Abstract**

2 Creating additional value out of biogas during waste treatment has become a priority in
3 past years. Biogas bioconversion into valuable bioproducts such as biopolymers has
4 emerged as a promising strategy. This work assessed the operational feasibility of a
5 bubble column bioreactor (BCB) implemented with gas recirculation and inoculated
6 with a polyhydroxybutyrate (PHB)-producing strain using biogas as substrate. The BCB
7 was initially operated at empty bed residence times (EBRTs) ranging from 30 to 120
8 min and gas recirculation ratios (R) from 0 to 30 to assess the gas-to-liquid mass
9 transfer and bioconversion of CH₄. Subsequently, the BCB was continuously operated
10 at a R of 30 and an EBRT of 60 min under excess of nitrogen and nitrogen feast-famine
11 cycles of 24h:24h to trigger PHB synthesis. Gas recirculation played a major role in
12 CH₄ gas-liquid transfer, providing almost fourfold higher CH₄ elimination capacities
13 (~41 g CH₄ m⁻³ h⁻¹) at the highest R and EBRT of 60 min. The long-term operation
14 under N excess conditions entailed nitrite accumulation (induced by O₂ limiting
15 conditions) and concurrent methanotrophic activity inhibition above ~60 mg N-NO₂⁻ L⁻¹.
16 ¹. Adjusting the N-NO₃⁻ supply to match microbial N demand successfully prevented
17 nitrite accumulation. Finally, the N feast-famine 24h:24h strategy supported a stable
18 CH₄ conversion with a removal efficiency of 70% along with a continuous PHB
19 production, which yielded PHB accumulations of 14.5 ± 2.9% (mg PHB mg⁻¹ total
20 suspended solids × 100). These outcomes represent the first step towards the integration
21 of biogas biorefineries into conventional anaerobic digestion plants.

22

23 **Keywords:** bioplastics; biorefinery; gas-liquid mass transfer; methane conversion;
24 methanotrophic bacteria; polyhydroxyalkanoate production

25 **Abbreviation list:**

26 BCB: bubble column bioreactor

27 CH₄-EC: methane elimination capacity

28 CH₄-RE: methane removal efficiency

29 EBRT: empty bed residence time

30 MOB: methane oxidizing bacteria

31 MSW: municipal solid waste

32 NMS: nitrate mineral salt medium

33 PCO₂: volumetric carbon dioxide production rate

34 PHAs: polyhydroxyalkanoates

35 PHB: poly-3-hydroxybutyrate

36 TN: total nitrogen

37 TSS: total suspended solids

38 R: gas recirculation ratio

39

40

41

42

43

44

45

46 **1. Introduction**

47 Polyhydroxyalkanoates (PHAs), which exhibit similarity in their mechanical
48 properties to polypropylene and polyethylene, are regarded as an attractive alternative
49 for replacing oil-based plastics due to the striving necessity of meeting the increasing
50 societal demand for more environmentally friendly materials (Lee & Na, 2013). These
51 renewable biopolyesters, with the added advantages of biocompatibility and
52 biodegradability, are synthesized intracellularly as carbon and energy storage by a broad
53 collection of microorganisms under nutrient deprivation and carbon surplus conditions
54 (Castilho et al., 2009; Myung et al., 2017; Narancic et al., 2018). Although the market
55 size of PHA is foreseen to quadruple by 2023, it is still relatively small. Indeed, PHA
56 represented only 1.4% of the global biopolymer market by 2018, which accounted for
57 2.1 million tonnes (European Bioplastics, 2018). Its expansion is currently hampered by
58 the significant contribution of the carbon feedstock (usually sugars, vegetable oils and
59 fatty acids) acquisition to the total production costs (up to 50%) (Koller et al., 2017).
60 Thus, PHAs prices (4 to 20 € kg⁻¹) are nowadays up to fifteen-fold higher than those of
61 their fossil counterparts (Blunt et al., 2018; Cantera et al., 2018).

62 On this scenario, the use of industrial by-products or wastes such as biogas as a
63 feedstock represents an opportunity to decrease the cost of PHAs production (Cal et al.,
64 2016; Strong et al. 2016). Biogas resulting from the anaerobic decomposition of the
65 biodegradable fraction of organic waste in anaerobic digestion plants or landfills is
66 primarily made up of methane (30-70%), carbon dioxide (20-50%) and hydrogen
67 sulfide (< 2%) (Nikiema et al., 2007; Muñoz et al., 2015). Gasification and methanation
68 of wood or recalcitrant organic waste can also generate a biomethane with CH₄
69 concentration higher than 90% (IEA, 2018). Methane, aside from being a potent
70 greenhouse gas, has been traditionally regarded as a green energy vector and is

71 increasingly used as a C source in industrial biotechnology. Indeed, the integration of
72 biogas into biorefineries for manufacturing high added value bioproducts such as PHA,
73 protein or ectoine is increasingly drawing attention due to the recent stabilization of the
74 biogas industry expansion (Mühlemeier et al., 2018).

75 PHA biosynthesis from CH₄ relies on the ability of type II-methane oxidizing
76 bacteria (MOB), also referred as methanotrophs, to synthesize PHA granules under
77 growth limiting conditions (Pieja et al., 2011a; Rostkowski et al., 2013; Zhang et al.,
78 2017). Type II-MOB metabolize methane and one-carbon compounds via the serine
79 cycle (Pieja et al., 2011a). When methane is used as the sole C and energy feedstock,
80 cells naturally synthesize the short-chain-length PHA poly-3-hydroxybutyrate (PHB).
81 Among type II-methanotrophs, the strain *Methyloscystis hirsuta* CSC1 has drawn
82 interest due to its high PHB-accumulating ability and metabolic plasticity (Bordel et al.,
83 2019b). In a recent work, López et al. (2018) obtained comparable cell growth and PHB
84 accumulation (43%) when synthetic biogas rather than CH₄ was used as carbon source
85 in *M. hirsuta* regardless of the presence of hydrogen sulfide. Nevertheless, to the best of
86 the authors' knowledge, the potential of biogas as a feedstock for the continuous
87 production of PHB and the constraints associated to a long-term continuous operation
88 have not been yet reported.

89 The major operational constraint associated to CH₄/biogas bioconversion
90 technologies is the poor mass transfer of O₂ and CH₄ (Henry's law constants (k_H) of
91 $1.3 \cdot 10^{-3}$ and $1.4 \cdot 10^{-3}$ M atm⁻¹ at standard conditions, respectively) (Sander, 2015). In
92 this regard, turbulent contactors such as bubble column bioreactors (BCBs) engineered
93 with innovative gas-liquid mass transfer strategies (i.e. the utilization of a non-aqueous
94 phase or the implementation of internal gas recirculation) can support an enhanced
95 methane biodegradation (Cantera et al., 2016; Rocha-Rios et al., 2011). Moreover, this

96 type of suspended-growth bioreactors allows an easy biomass harvesting and bioproduct
97 downstream processing (López et al., 2019).

98 This study aims at optimizing the biogas residence time and the internal
99 recirculation rate to maximize CH₄ mass transfer and at assessing the long-term (> 4
100 weeks of stable operation) production of PHB from biogas by *M. hirsuta* in a
101 continuous BCB equipped with gas recirculation.

102 **2 Materials and methods**

103 To fulfill the above-mentioned objectives, the experimental research was structured
104 into two main assays that were carried out in a bubble column bioreactor whose
105 configuration was described in section 2.2.1. A first approach pursued the optimization
106 of operating parameters through a mass transfer test in which 18 different conditions for
107 EBRT and R (2.2.2) were assayed. A second approach aimed at investigating the
108 process stability (2.2.3) under non-nutrient limited conditions prior the implementation
109 of sequential nitrogen feast-famine cycles (2.2.4) to induce the PHB synthesis. Sections
110 2.2.3 and 2.2.4 were performed at the same EBRT and R conditions.

111 **2.1 Chemicals, culture media and inoculum**

112 **2.1.1 Chemicals.** The chemicals used for PHB extraction (trichloromethane (≥ 99%), 1-
113 propanol (99.7%), benzoic acid (≥ 99.5%), and hydrochloric acid (37% w/v)) and for
114 the culture medium preparation were acquired from PanReac AppliChem (Spain),
115 except KNO₃, which was purchased from COFARCAS (Spain). Poly(3-
116 hydroxybutyrate-co-3-hydroxyvalerate) (PHBV) with a mole fraction 3HB/3HV of
117 88/12 (≥ 99.99%) was acquired from Sigma-Aldrich (USA). O₂ (≥ 99.5%), CH₄ (≥

118 99.995%), He ($\geq 99.5\%$), and a synthetic biogas mixture containing 70% of CH₄ and
119 30% of CO₂ were provided by Abelló Linde S.A. (Spain).

120 **2.1.2 Culture medium.** Unless otherwise specified, a nitrate mineral salt (NMS)
121 medium containing the following macronutrients (g L⁻¹) was employed: 0.2
122 CaCl₂·2H₂O, 1.0 KNO₃, 1.1 MgSO₄·7H₂O and the following trace elements (mg L⁻¹):
123 0.01 NiCl₂·6H₂O, 0.02 MnCl₂·4H₂O, 0.03 CoCl₂, 0.015 H₃BO₃, 0.38 Fe-EDTA, 0.3
124 Na₂EDTA·2H₂O, 0.4 Na₂MoO₄·2H₂O, 0.4 ZnSO₄·7H₂O, 0.5 FeSO₄·7H₂O and 1.0
125 CuSO₄·5H₂O. The NMS was stored in borosilicate glass bottles and autoclaved (121 °C,
126 30 min). After cooling the sterile NMS down to room temperature, 10 mL of a sterile
127 buffer solution (72 g L⁻¹ Na₂HPO₄·12H₂O and 26 g L⁻¹ KH₂PO₄) per liter of NMS
128 medium were added to adjust its pH to 6.8.

129 **2.1.3 Strain and inoculum preparation.** A stock culture of *Methylocystis hirsuta*
130 CSC1 (DSM 18500) was purchased from Leibniz-Institut DSMZ (Germany) and stored
131 at 4°C until use. The cultivation of *M. hirsuta*, which was grown up to a concentration
132 of 0.54 ± 0.03 g L⁻¹ prior to inoculation of the bioreactors, was conducted in two stages
133 under strictly sterile conditions based on López et al. (2018) procedure. Initially,
134 gastight serum vials of 125 mL containing 50 mL of NMS medium were inoculated
135 from the DSMZ vial at 10% (v v⁻¹) under an O₂:CH₄ atmosphere (66.7:33.3% (v v⁻¹)).
136 The cultures were incubated in an orbital shaker at 200 rpm and 30°C for 8 days. Once
137 the cultures were metabolically active, the headspace atmosphere was restored
138 systematically up to a maximum of 5 times every 24 h. To that end, filtered oxygen was
139 gassed for 5 min and replaced (25 mL) with methane afterwards with a 50 mL gastight
140 syringe (Hamilton 1050 TLL, USA). Finally, aliquots of 10 mL of this active culture
141 were transferred to sterile serum bottles (2.2 L) containing 0.4 L of NMS medium
142 sealed with aluminum caps and chlorobutyl rubber stoppers under an O₂:CH₄:CO₂

143 atmosphere of 58.3:29.2:12.5% (v v⁻¹). The headspace atmosphere was obtained by
144 flushing for 3 min a gas mixture composed of biogas and oxygen with the above
145 mentioned composition from a 100 L-Tedlar gas sampling bag (Sigma-Aldrich, USA).
146 The cultures were grown under continuous stirring at 300 rpm (Thermo Scientific
147 Variomag Multipoint 6, USA) and 25°C in a thermostated room for 10-12 days until
148 complete methane depletion.

149

150 **2.2 Experimental procedure**

151 **2.2.1 Experimental set-up**

152 The study herein presented was carried out in a bench-scale bubble column
153 bioreactor (BCB) implemented with gas recirculation to ensure a high CH₄ and O₂ mass
154 transfer to the cultivation broth (**Fig. 1**). The bioreactor, with a working volume of 2.5
155 L, was equipped with a set of three micropore stainless steel diffusers (2 μm, Supelco,
156 USA) and a magnetic stirrer (Agimatic S, JP Selecta, Spain, 500 rpm) located at the
157 bottom of the column to ensure an adequate mixing throughout the column. A gas
158 mixture composed of atmospheric air and synthetic biogas was continuously sparged
159 into the bioreactor through the diffusers. The biogas stream was regulated by a mass
160 flow controller (GFC17, AalborgTM, USA), whereas the atmospheric air was supplied
161 by an air compressor and controlled by a rotameter to deliver a gas mixture with O₂:CH₄
162 ratios ranging from 1.5:1 to 2:1. A condenser (maintained at 10°C) was installed at the
163 internal gas recirculation line in order to prevent operational problems derived from
164 water condensation. The BCB was operated at 25°C in a temperature-controlled room.

165

<Figure 1>

166

167 **2.2.2 CH₄/O₂ mass transfer optimization test.**

168 The bioreactor was first inoculated with a fresh *Methylocystis hirsuta* CSC1 culture
169 resulting in an initial total suspended solids (TSS) concentration of 0.5 g L⁻¹. The BCB
170 was initially operated at an EBRT of 30 min with a CH₄ content of 90 ± 8 g CH₄ m⁻³ (14
171 ± 1 % v v⁻¹) and without gas recirculation for four weeks. In this period, biomass
172 concentration reached 3 g L⁻¹, a concentration that was maintained under all operational
173 conditions tested to guarantee that the process was not biologically limited. For this
174 purpose, aliquots of 500 mL of culture broth from the BCB were daily centrifuged
175 (10000 rpm, 8 min) and replaced by fresh NMS. In order to maintain a constant biomass
176 concentration of ~3.5 g TSS L⁻¹ in the culture broth, the harvested biomass was either
177 partially returned to the system or discarded. The diffusers were replaced when the
178 pressure drop exceeded 0.5 bar. The nitrogen concentration of the NMS supplied was
179 adjusted from 1 to 7 g L⁻¹ KNO₃ at each operational condition tested to avoid nitrogen
180 limitation in the culture broth. Subsequently, the influence of the EBRT and the gas
181 recirculation ratio (hereinafter referred to as R) on CH₄ biodegradation under balanced
182 growth conditions was assessed (**Table 1**). Each operational condition was maintained
183 for a period of 5-8 days, which ensured steady state operation regarding the liquid and
184 gas phases.

185

186

187

< **Table 1** >

188

189

190

191 **2.2.3 Methane biodegradation under nitrogen surplus conditions in the BCB**

192 The bioreactor was inoculated with the above mentioned strain at 90 ± 10 mg TSS
193 L^{-1} and operated under the optimum operational conditions selected in the previous test
194 (EBRT of 60 min, $R = 30$, methane inlet load of 68 ± 8 g $CH_4 m^{-3} h^{-1}$ and an $O_2:CH_4$
195 molar ratio of 1.8 ± 0.3) in order to identify long-term microbial and mechanical
196 limitations during continuous CH_4 abatement. Thus, CH_4 biodegradation was
197 investigated under nitrogen excess for 50 days (from day 0 to day 35, and from day 51
198 to day 66) and nitrogen limiting conditions for 15 days (from day 36 to day 50) using a
199 modified NMS medium with $N-NO_3^-$ concentrations of 552 and 276 mg L^{-1} ,
200 respectively. During the first week of operation, the biomass contained in 500 mL of
201 culture broth was daily collected and returned to the BCB re-suspended into 500 mL of
202 fresh NMS. From day 8 onwards, no biomass was returned to the BCB so that the
203 biomass concentration was maintained at ~ 3 g L^{-1} .

204 **2.2.4 Biogas utilization coupled to continuous PHB production in the BCB**

205 This test aimed at assessing the continuous PHB biosynthesis from biogas by *M.*
206 *hirsuta*. The system was initially inoculated at 190 ± 0 mg TSS L^{-1} with *M. hirsuta* and
207 operated at an EBRT of 60 min, a R of 30 and a methane inlet load of 60 ± 3 g $CH_4 m^{-3}$
208 h^{-1} (corresponding to an $O_2:CH_4$ ratio of 2.1 ± 0.1). CH_4 biodegradation was initially
209 investigated under nitrogen-balanced conditions for 32 days of operation (using a NMS
210 with a $N-NO_3^-$ content of 345 mg L^{-1}). By day 33, a nitrogen-free mineral salt (NFMS)
211 medium was supplied to deplete the nitrogen in the BCB, and subsequently 15
212 sequential nitrogen feast-famine cycles of 48 h (i.e. 24 h under nitrogen balanced
213 growth conditions followed by 24 h under nitrogen starvation) were applied to trigger
214 PHB biosynthesis. To this end, 500 mL d^{-1} of modified NMS medium (345 mg $N-NO_3^-$

215 L⁻¹) or NFMS medium were alternatively provided corresponding to a dilution rate of
216 0.2 d⁻¹.

217 Gas flow rate, pressure drop in the gas diffusers and gas composition in the inlet and
218 outlet streams (CH₄, CO₂ and O₂) were monitored daily. Total dissolved nitrogen (TN),
219 NO₂⁻ and NO₃⁻ in the culture broth were also recorded. Culture samples (40 mL) were
220 collected for the determination of TSS, pH and PHAs. The pellets from the
221 centrifugation of 3 mL of culture broth samples (10000 rpm, 10 min) were stored at -
222 20°C prior PHAs analysis.

223 **2.3 Analytical procedures**

224 CH₄, CO₂ and O₂ gas concentrations were measured in duplicate in a gas
225 chromatograph coupled with a thermal conductivity detector (Bruker 430, Bruker
226 Corporation, USA) and equipped with CP-Molsieve 5A and CP-PoraBOND Q columns.
227 The pressure drop in the BCB was monitored with a pressure sensor (PI1696, Ifm
228 Electronic, Germany). Outlet gas flow rate was estimated by using the water
229 displacement method.

230 Biomass concentration, expressed as TSS, was determined according to the 2540
231 method (APHA, 2017) using 0.45 µm pore size filters (Merck, Germany). Biomass
232 density was also estimated using optical density measurements at 600 nm with a UV-
233 2550 spectrophotometer (Shimadzu, Japan). A Basic 20 pH meter (Crison, Spain) was
234 used for the measurement of pH.

235 NO₂⁻ and NO₃⁻ concentrations were analyzed by ion chromatography using a Waters
236 432 HPLC conductivity detector (Waters Corporation, USA). TN and total organic
237 carbon (TOC) concentrations were quantified simultaneously in a TOC-V analyzer
238 equipped with a Shimadzu TNM-1 unit.

239 The biopolymer extraction procedure for PHB quantification via gas
240 chromatography-mass spectrometry (GC-MS) was conducted according to Rodríguez et
241 al. (2020).

242 **2.4 Calculation**

243 **2.4.1 Performance indicators of the BCB**

244 The elimination capacity ($CH_4 - EC$), removal efficiency ($CH_4 - RE$) and the
245 volumetric carbon dioxide production rate (PCO_2) are defined as:

$$246 \quad CH_4 - EC = \frac{Q \cdot (C_{CH_4, in} - C_{CH_4, out})}{V_R} \quad (\text{Eq.1})$$

$$247 \quad CH_4 - RE (\%) = \frac{C_{CH_4, in} - C_{CH_4, out}}{C_{CH_4, in}} \times 100 \quad (\text{Eq.2})$$

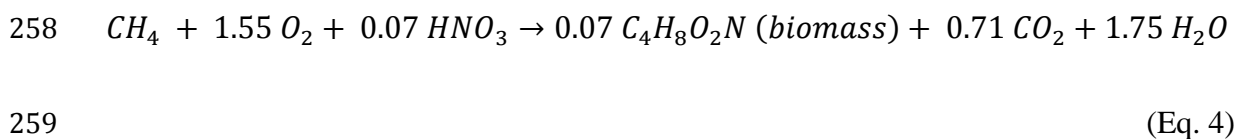
$$248 \quad PCO_2 = \frac{Q \cdot (C_{CO_2, out} - C_{CO_2, in})}{V_R} \quad (\text{Eq.3})$$

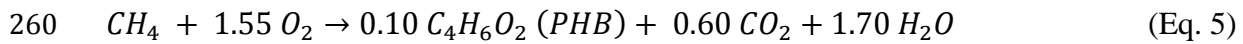
249 where C_{in} and C_{out} are the inlet and outlet concentration (g m^{-3}), respectively, Q is the
250 inlet gas flow ($\text{m}^3 \text{h}^{-1}$) and V_R (m^3) is the working volume of the bioreactor.

251 **2.4.2 Stoichiometry and theoretical PHB productivity in the BCB**

252 According to literature, the theoretical biomass and PHB yields in type-II
253 methanotrophs are $0.46 \text{ g biomass g}^{-1} \text{ CH}_4$ (using nitrate as nitrogen source) (Asenjo
254 and Suk, 1986) and $0.54 \text{ g PHB g}^{-1} \text{ CH}_4$, respectively (Yamane, 1993; Khosravi-Darani
255 et al., 2013).

256 The overall equations for biomass growth and PHB accumulation supporting these
257 yields are given below.





261 The sum of Eq. 1 and Eq.2 taking into consideration the duration of both growth and
 262 accumulation phases within the cycles (1/2) gives the theoretical PHB yield (Y_{PHB}^{th}) of
 263 the global process.

264 Thus, the theoretical PHB productivity (P_{th}) for a 24h:24h growth:accumulation cycle
 265 was estimated using the following formula:

266 $P_{PHB}^{th} (kg m^{-3} d^{-1}) = \frac{(1/2) \cdot 0.54 \cdot CH_4EC \cdot 24 (h/d)}{1000 (g/kg)}$ (Eq. 6)

267 where 0.54 is the Y_{PHB}^{th} (g PHB produced g^{-1} CH_4 removed) and CH_4EC is the methane
 268 elimination capacity ($g CH_4 m^{-3} h^{-1}$).

269

270 **3 Results and discussion**

271 **3.1 CH_4 mass transfer optimization in the BCB: Influence of the empty bed** 272 **residence time and the gas recirculation on CH_4 degradation**

273 BCB operation at EBRTs of 30, 60 and 120 min with no internal gas recirculation
 274 showed CH_4 -elimination capacities (CH_4 -ECs) of 29.8 ± 2.0 , 11 ± 1.7 and 6.9 ± 1.8 g
 275 $CH_4 m^{-3} h^{-1}$, with associated CH_4 -removal efficiencies (CH_4 -REs) of 13.3 ± 0.6 , $12.3 \pm$
 276 1.7 and $12.7 \pm 1.2\%$, respectively (**Fig. 2a and 2b**). This suggests that the enhancement
 277 in the turbulence of the cultivation broth mediated by the decrease in the EBRT caused
 278 a positive effect on the volumetric mass transfer coefficient (K_{LaCH_4}) and consequently,
 279 on the CH_4 -EC.

280 Internal gas recirculation has been reported as a promising strategy for enhancing
 281 CH_4 -biodegradation in biotrickling filters (> 2.5 times) and BCBs (> 2.1 times) during

282 the treatment of CH₄-diluted air emissions (Estrada et al., 2014; García-Pérez et al.,
283 2018). This approach allows decoupling the actual gas residence time in the reactor
284 from the liquid turbulence in the bioreactor. Thus, at an EBRT of 30 min, the CH₄-EC
285 increased to 42.2 ± 1.0, 55.1 ± 1.7, 54.3 ± 1.6, 57.6 ± 1.4 and 73.8 ± 2.1 g CH₄ m⁻³ h⁻¹ at
286 R of 2.5, 5, 10, 15 and 30, respectively (**Fig. 2a**). Consequently, CH₄-REs increased to
287 20.5 ± 0.8, 25.0 ± 1.4, 27.1 ± 3.5, 32.7 ± 2.0 and 39.0 ± 3.6% at these R values (**Fig.**
288 **2b**). Similarly, Rocha-Rios et al. (2011) reported an enhancement of 51% in the CH₄
289 biodegradation performance of an airlift loop bioreactor by increasing the gas
290 recirculation rate from 0 to 1 volumes per minute (vvm).

291 At EBRTs of 60 and 120 min, the CH₄-EC increased by a factor of 3.7 (from 11.0 ±
292 1.7 to 41.1 ± 0.4 g CH₄ m⁻³ h⁻¹) and 3.2 (from 6.9 ± 1.8 to 22.2 ± 0.7 g CH₄ m⁻³ h⁻¹),
293 respectively (**Fig. 2b**), at the highest R applied. A similar behavior was observed during
294 the biodegradation of CH₄-laden emissions (4% v v⁻¹) in a BCB with internal gas
295 recirculation. However, the lower CH₄ gas-liquid gradients during the biodegradation of
296 diluted CH₄ emissions resulted in lower CH₄-ECs (i.e.: 35.2 ± 0.4 g CH₄ m⁻³ h⁻¹ at an
297 EBRT of 30 and R of 15) (García-Pérez et al., 2018).

298 < **Figure 2** >

299 It can be inferred that internal gas recirculation induces opposite effects by
300 increasing system turbulence at the expense of reducing CH₄ gas-liquid gradient in the
301 column. Results in **Fig. 3** indicates that shorter gas contact times in the system mediated
302 greater elimination capacities despite the negative effects which may be associated to a
303 high turbulence such as bubble coalescence or *eddies* (Stone et al., 2017). The
304 correlation observed is explained by the fact that the input of energy into the system
305 reduces the liquid film and enhance the superficial contact area by breaking the bubbles
306 (Kraakman et al., 2011). For instance, the operation of the BCB in the absence of gas

307 recirculation at an EBRT of 30 min and at an EBRT of 120 min with R of 2.5 showed
308 similar virtual EBRTs (30 and 34.3 min, respectively), but a different CH₄-degradation
309 performance with ECs of 29.8 ± 2.0 and 11.7 ± 0.5 g CH₄ m⁻³ h⁻¹ and CH₄-REs of 13.3
310 ± 0.6 and $23.1 \pm 1.5\%$, respectively.

311 **<Figure 3>**

312 Overall, the elimination capacities herein recorded were superior to the ~ 20 g m⁻³
313 h⁻¹ achieved in an internal loop airlift reactor (Rocha et al., 2011). Furthermore, there
314 was a satisfactory match with the ~ 75 and 22 g m⁻³ h⁻¹ (REs of 34 and 15%) achieved in
315 a stirred tank reactor (at 800 rpm) and a trickling bed reactor both operated with a
316 similar methane load. Conversely, the supplementation of the stirred tank reactor with
317 10% silicon oil resulted in a higher EC (106 g m⁻³ h⁻¹) than the maximum EC reached
318 in this work (74 g m⁻³ h⁻¹) (Rocha et al., 2009). Despite having proved to enhance the
319 gas-liquid transfer at high stirring rates in turbulent contactors (Kraakman et al., 2011),
320 the addition of a non-aqueous phase is up to date not suitable for biomass valorization
321 (Stone et al., 2017).

322 The highest CH₄-REs were targeted as selection criteria in order to maximize the
323 utilization of CH₄ from biogas as a substrate for PHB biosynthesis (Pérez et al., 2019).
324 Therefore, EBRTs of 60 and 120 min with R of 30 exhibited the highest potential for
325 CH₄ bioconversion with CH₄-REs of 45.1 ± 1.2 and $47.8 \pm 3.5\%$ and CH₄-ECs of $41.1 \pm$
326 0.4 and 22.2 ± 0.7 g CH₄ m⁻³ h⁻¹, respectively. In the light of the similar CH₄-REs at
327 both EBRTs, the operation at an EBRT of 60 min with a R of 30 was selected as the
328 most appropriate condition for PHB production given the higher CH₄-EC, which would
329 ultimately result in a significant reduction of equipment costs and enhanced bioreactor
330 productivities. This selection was also supported by a carbon footprint analysis (**Fig.**

331 **S2**), in which the selected operating conditions mediated the largest CO₂ equivalents
332 reduction (30%) compared to a scenario where the biogas was vented.

333 The mass transfer experiments here presented were performed with a sufficiently
334 high biomass concentration (>3 g TSS L⁻¹) to guarantee that CH₄ gas-liquid mass
335 transfer was the limiting step of the process. Likewise, the high dilution rate applied
336 prevented nutrient-limiting conditions and secondary metabolites accumulation, which
337 could negatively affect CH₄ biodegradation performance. In this regard, the minimum
338 TN (41.56 ppm) and maximum TOC (74.6 ppm) concentrations corresponded to the
339 maximum CH₄-ECs achieved at an EBRT of 30 min and R of 30. Accordingly, the CH₄
340 mineralization ratio, expressed as the volumetric CO₂ production rate to methane
341 elimination capacity ratio (PCO₂/CH₄-EC), remained constant at 2.4 ± 0.2, 2.2 ± 0.2 and
342 2.4 ± 0.3 at EBRTs of 30, 60 and 120 min, respectively, which suggested a balanced
343 methanotrophic metabolism along the entire experiment.

344 **3.2 Effect of the N supply on the continuous CH₄ abatement**

345 The CH₄-EC rapidly increased up to 53.0 ± 2.3 g CH₄ m⁻³ h⁻¹ concomitantly with an
346 increase in PCO₂ up to 119.9 ± 0.1 g CO₂ m⁻³ h⁻¹ following BCB inoculation (**Fig. 4a**).
347 Both CH₄-EC and PCO₂ remained stable at 57.1 ± 3.6 g CH₄ m⁻³ h⁻¹ and 128.7 ± 11.4 g
348 CO₂ m⁻³ h⁻¹, respectively, during the first 20 days. Biomass concentration increased up
349 to 4.8 ± 0.1 g L⁻¹ by day 8 and steadily decreased to 2.4 ± 0.0 g L⁻¹ by day 20 (**Fig 4c**).
350 Unexpectedly, CH₄-EC and PCO₂ experienced a slight decrease by day 20 (**Fig. 4a**).

351 Thus, all biomass was collected by centrifugation and resuspended into fresh NMS
352 medium on day 23 to prevent the culture from a potential accumulation of non-desired
353 metabolites. Despite the system showed an almost complete recovery within the two
354 next days, a sharp drop in CH₄ biodegradation performance occurred again. A new

355 steady state with CH₄-EC of $7.4 \pm 1.5 \text{ g CH}_4 \text{ m}^{-3} \text{ h}^{-1}$ and PCO₂ of $21.5 \pm 4.2 \text{ g CO}_2 \text{ m}^{-3}$
356 h⁻¹ was recorded from day 26 to 36 concomitantly with a gradual biomass wash-out
357 (**Fig. 4c**).

358 The BCB was reinoculated by day 36 with *M. hirsuta* resuspended into NMS
359 medium prepared with half of the nitrogen concentration ($276 \text{ mg N-NO}_3^- \text{ L}^{-1}$). As
360 shown in **Fig. 4a**, a consistent steady state was rapidly achieved and maintained for the
361 next 14 days under no excess of nitrogen. When the N-NO₃⁻ concentration of the NMS
362 medium was restored to $552 \text{ mg N-NO}_3^- \text{ L}^{-1}$, and the system was no longer nitrogen
363 limited, the CH₄-EC remained constant for four days and eventually dropped from 41.1
364 ± 2.7 to $5.2 \pm 0.7 \text{ g CH}_4 \text{ m}^{-3} \text{ h}^{-1}$. PCO₂ was correlated to CH₄-EC with a mineralization
365 of $79.2 \pm 7.6\%$ during both steady states achieved.

366 < **Figure 4** >

367 The analysis of the N species prevailing in the cultivation broth revealed that nitrate
368 reduction to nitrite occurred from day 11 onwards, resulting in nitrite accumulation in
369 the liquid broth, with a maximum concentration of $83.3 \text{ mg N-NO}_2^- \text{ L}^{-1}$ by day 22. It can
370 be inferred that nitrite accumulation (mediated by the O₂ limiting conditions in the
371 cultivation broth at the low O₂:CH₄ ratios used; 1.3:1-1.7:1) induced the inhibition of
372 the methanotrophic metabolism, leading to a deterioration of the system performance
373 despite the high NMS medium dilution rate applied (0.2 d^{-1}). Nitrite formation rapidly
374 occurred again along with a decrease in CH₄-EC after biomass resuspension into fresh
375 NMS medium. Interestingly, when N supply was limited from day 36 to day 50, this
376 accumulation did not occur, which allowed maintaining a stable process operation
377 throughout this period. By day 51, the increase in N loading triggered again the
378 accumulation of nitrite. This confirmed that nitrite accumulation and process inhibition
379 was inherent to N surplus conditions.

380 In this context, the batchwise cultivation of *M. hirsuta* CSC1 in mineral salt medium
381 prepared with nitrite as a nitrogen source (138 mg N-NO₂⁻ L⁻¹) resulted in a complete
382 growth inhibition (Rodríguez et al., 2020). The inhibitory effect of nitrite in type II-
383 MOB was already reported in a previous study, where *Methylocystis* sp. growing in both
384 nitrate- and ammonium-containing growth medium increased its doubling time by 65
385 and 51%, respectively, when supplemented with 2.5 mM NaNO₂ (35 mg N-NO₂⁻ L⁻¹)
386 (Nyerges et al., 2010). Conversely, the type I strain *Methyломicrobium album*
387 maintained similar doubling times and CH₄ removal rates to those of the control tests
388 under identical conditions, with additional nitrous oxide production. Interestingly, the
389 genome sequence of *Methylocystis hirsuta* CSC1 recently elucidated revealed that this
390 strain possesses the mechanisms to conduct partially the denitrification pathway (Bordel
391 et al., 2019a). To the best of the author's knowledge, this phenomenon has not been
392 previously reported in continuous bioreactors devoted to methane abatement. In this
393 regard, N supply limitation strategies can overcome this concurrent nitrite accumulation
394 while inducing PHB synthesis in *M. hirsuta* (Rodríguez et al., 2020).

395 Finally, the pH of the cultivation broth during the stationary states achieved (7.2 ±
396 0.1) suggests that the oxidation of methane releases basic metabolites that maintained
397 the pH above the pH of the mineral salt medium (6.8 ± 0.1) despite the presence of
398 buffer and the solubilization of the CO₂ inherently present in biogas.

399

400 **3.3 Biogas utilization coupled to continuous PHB production in the BCB**

401 The BCB was continuously operated under the optimum operational parameters
402 determined in the previous tests (EBRT of 60 min, R of 30 and a N supply of 69 mg N-
403 NO₃⁻ d⁻¹ L⁻¹) to achieve a steady CH₄ abatement along with a simultaneous biopolymer

404 production. Within the first two days of operation, the system achieved a stable CH₄-EC
405 of $40.2 \pm 2.3 \text{ g CH}_4 \text{ m}^{-3} \text{ h}^{-1}$ corresponding to a CH₄-RE of $70.1 \pm 2.7\%$ (**Fig. 5a**). These
406 CH₄-EC values, which are in accordance with those achieved during the CH₄/O₂ mass
407 transfer test under comparable operational conditions ($41.1 \pm 0.4 \text{ g CH}_4 \text{ m}^{-3} \text{ h}^{-1}$),
408 supported a PCO₂ of $78.5 \pm 6.3 \text{ g CO}_2 \text{ m}^{-3} \text{ h}^{-1}$ along with a mineralization of $70.5 \pm$
409 4.7% . As discussed in Section 3.1, the performance indicators of this study were
410 comparable to those typically reported for poorly water soluble compounds ($< 70\%$)
411 (Kraakman et al., 2011).

412 Additionally, the observed O₂:CH₄ molar consumption at this stage was 1.5 ± 0.1 ,
413 which corresponded to the theoretical value (~ 1.5 - 2) reported by Karthikeyan et al.
414 (2015). The pH remained stable at 7.2 ± 0.2 throughout the whole operation and the
415 presence of nitrite was not detected, thus avoiding culture inhibition (**Fig. 5b**). This
416 supports the hypothesis that dissimilatory nitrate reduction, where NO₃⁻ is used as the
417 electron acceptor for energy production, did not prevail over assimilatory nitrate
418 reduction when N consumption and N supply are balanced. These outcomes have
419 important implications for the application of this biotechnology at pilot or industrial
420 scale under long-term operation. Biomass concentration was maintained at $3.0 \pm 0.9 \text{ g}$
421 TSS L^{-1} from day 10 onwards, accounting for a biomass production of $20.0 \pm 8.3 \text{ g TSS}$
422 $\text{m}^{-3} \text{ h}^{-1}$ (**Fig. 5c**).

423 Process operation under sequential N feast-famine cycles from day 35 onward
424 supported a stable CH₄-EC of $40.5 \pm 1.4 \text{ g CH}_4 \text{ m}^{-3} \text{ h}^{-1}$ over 15 cycles. Remarkably, the
425 N starvation periods (24 h) did not entail a significant decrease in the system
426 performance as previously reported by García-Pérez et al. (2018). These authors
427 observed a deterioration in the EC from the fifth cycle onwards when longer N
428 deprivation periods were applied (48 h) during the treatment of diluted CH₄ emissions

429 in a BCB. Interestingly, an increase in the mineralization ratio (from 2.1 ± 0.1 to $2.3 \pm$
430 $0.1 \text{ g CO}_2 \text{ g}^{-1} \text{ CH}_4$) was recorded during the N-deprivation periods (**Fig 5a**), which
431 suggested a higher carbon flux towards formaldehyde oxidation to CO_2 for the
432 regeneration of reducing equivalents needed in the PHB pathway (Khosravi-Darani et
433 al., 2013).

434 The implementation of feast-famine N cycles was initiated after a first limitation
435 period lasting 48 h, which induced a PHB accumulation up to $23.2 \pm 0.3\%$ (mg PHB
436 $\text{mg}^{-1} \text{ TSS} \times 100$) in the cells. **Fig 5b** illustrates the dynamics of N addition and rapid N
437 uptake by *M. hirsuta* during the 15 cycles. The implementation of 15 N feast-famine
438 cycles supported an average PHB accumulation of $14.5 \pm 2.9\%$ (**Fig. 5c**). The
439 determination of the partitioning coefficients revealed that most of the electrons derived
440 from methane were used for energy production by the cells ($f_e = 0.80$) during the
441 accumulation phase (**Table S1**). Although values ranging 0.52-0.94 were reported by
442 López et al. (2018) when cultures were supplemented with volatile fatty acids, the f_e
443 found in batch assays were typically lower (~ 0.32). During each cycle, the presence of
444 N in the cultivation broth triggered the co-consumption of PHB and CH_4 , which
445 entailed a decrease of $\sim 5\%$ in PHB accumulation (up to $9.1 \pm 3.5\%$).

446 < **Figure 5** >

447 According to Bordel et al. (2019c), the depletion of the stored PHB in the
448 presence of both CH_4 and nitrogen occurs through anaplerotic reactions. These reactions
449 provide intermediates that are necessary for the synthesis of building blocks such as
450 glyoxylate and succinyl-CoA into the serine and TCA cycle, respectively. In this
451 context, a previous work demonstrated that the consumption of the accumulated PHB
452 by *Methylocystis parvus* did not support growth in the absence of CH_4 (Pieja et al.,

453 2011b). In fact, it has been reported that PHB storage in the presence of CH₄ could
454 provide bacteria a competitive advantage.

455 Repeated N cycles of 24-h in a sequencing batch reactor resulted in a similar
456 PHB content in a methanotrophic mixed culture (~15%) (Pieja et al., 2012). Although
457 the figures recorded were nearly a third than those achieved batchwise by *M. hirsuta*
458 using biogas as CH₄ source (up to 45%) (López et al., 2018; Rodríguez et al., 2020), no
459 previous study has been carried out under strictly continuous operation mode aiming at
460 biogas valorization. It must be emphasized that the carbon mass balance conducted
461 presented errors of 0.4 and 5.4% during the growth and accumulation phase,
462 respectively, which validated the results and analyses carried out (Table S1).

463 PHB productivities ranging from 0.04 to 0.06 kg PHB m⁻³ d⁻¹, corresponding to non-
464 N limited and N limiting conditions, respectively, were obtained. An estimation based
465 on the global stoichiometry of the process and the CH₄ uptake rate (Eq. 6) led to a
466 theoretical productivity value of ~0.26 kg PHB m⁻³ d⁻¹. The productivities herein
467 recorded remained below this value likely due to the substantial impact observed from
468 PHB consumption during the growth phase on the overall yield of the process. In this
469 regard, PHB consumption lowered this value nearly by 60%, i.e. from 0.12 (expected)
470 to 0.05 g PHB produced g⁻¹ CH₄ (Table S1). Thus, PHB depletion would result in a
471 PHB productivity of 0.10 kg PHB m⁻³ h⁻¹, which would match satisfactorily with the
472 experimental results. In addition, productivities slightly below the theoretical figures
473 could be also explained by the short time available for methanotrophs to accumulate
474 PHB during the N deprived period applied. A previous study using a similar gas-liquid
475 contactor in batch mode and natural gas as a CH₄ source found that the maximum PHB
476 accumulation (30.5%) occurred over 84 h (Rahnama et al., 2012). In this context, a
477 strategy with an extended N limiting period was carried out (24h with N:48 without N).

478 However, process operation with such long N limitation resulted in an EC and PHB
479 content decrease after the first complete cycle (data not shown), which ultimately
480 resulted in system collapse.

481 In a biorefinery context, in which a medium size municipal solid waste (MSW) plant
482 treats over 300 ton d⁻¹ of residues with an organic fraction of 46% (IEA Bioenergy), 1
483 ton of VS typically would yield 121.7 m³ CH₄. Thus, considering repeated N cycles of
484 24h:24h, a removal efficiency of 70% and a PHB yield of 0.54 g PHB g⁻¹ CH₄, it can be
485 predicted that 72.1 ton of MSW would be necessary for the production of 1 ton of PHB.
486 This is, 6.9 kg of PHB can be produced out of 1 ton of MSW. In this regard, a recent
487 geographical analysis conducted by Pérez et al. (2020) revealed that a combined
488 scenario, i.e. PHB and cogeneration from biogas, in countries in which energy costs are
489 high, would achieve PHB production costs as low as 1.5 euro kg⁻¹. It also came out that
490 in those regions where energy production is not economically favorable, biogas could
491 be fully exploited for PHB production with competitive production costs (4.1 euro kg⁻¹).

492 Finally, it is also worth mentioning that methane content in the exhaust gas from the
493 reactor was 3.0 ± 0.0 % v v⁻¹ as a result of the high dilution ratio when using air as O₂
494 source. Therefore, this CH₄ content would not match the minimum concentration
495 required for CH₄ combustion, which is above 35-40% (Haubrichs and Widmann, 2006).

496

497

498

499 **4 Conclusions**

500 This work demonstrated for the first time the technical feasibility of PHB
501 production from biogas in a continuous bubble column bioreactor equipped with
502 internal gas recirculation. This work provided valuable insights into the operational
503 conditions supporting a sustained CH₄ bioconversion into PHB. The implementation of
504 internal gas recirculation led to the decoupling of the turbulence in the cultivation broth
505 and gas EBRT, providing outstanding CH₄-ECs and CH₄-REs with values up to 4 times
506 higher than in the absence of gas recirculation. An EBRT of 60 min and a R of 30 were
507 identified as the optimal conditions for maximizing substrate utilization. N-NO₃⁻ supply
508 to the culture broth must match N demand when using biogas as a CH₄ source in order
509 to prevent nitrite accumulation and the subsequent inhibition of methanotrophic activity.
510 Finally, the N feast-famine strategy applied for PHB production (24h:24h) under
511 optimal mass transfer conditions conferred a stable CH₄ oxidation (stage I) and a
512 continuous PHB production (stage II) with a CH₄-RE of 70% and PHB productivities up
513 to 0.06 kg PHB m⁻³ d⁻¹. These findings highlight the potential of methanotrophic
514 bacteria as an effective/feasible platform for PHB production within a biogas bio-
515 refinery concept. Furthermore, the use of biogas as a low-cost and “green” alternative to
516 conventional carbon sources for biopolymer production would boost their viability in
517 terms of environmental and economic impact. Further studies should explore process
518 robustness under N limiting conditions ranging from 24 to 48 h to achieve higher PHB
519 accumulations.

520

521

522

523 **Acknowledgements**

524 This work was supported by the Spanish Ministry of Science and Innovation
525 (grant number BES-2016-077160, project CTM2015-70442-R). The Regional
526 Government of Castilla y León and the EU-FEDER programme (CLU 2017-09, UIC
527 071 and VA281P18) are also acknowledged. J.C. López, E. Marcos, A. Crespo and B.
528 Muñoz are gratefully acknowledged for their practical assistance.

529

530 **References**

- 531 APHA, 2017. Standard Methods for the Examination of Water and Wastewater. 23rd
532 ed, American Public Health Association. Washington, D.C.
- 533 Asenjo, J.A., Suk, J.S., 1986. Microbial Conversion of Methane into poly- β -
534 hydroxybutyrate (PHB): Growth and intracellular product accumulation in a
535 type II methanotroph. *J Ferment Technol*, 64(4), 271-278.
536 [https://doi.org/10.1016/0385-6380\(86\)90118-4](https://doi.org/10.1016/0385-6380(86)90118-4)
- 537 Blunt, W., Levin, B.D., Cicek, N., 2018. Bioreactor Operating Strategies for Improved
538 Polyhydroxyalkanoate (PHA) Productivity. *Polymers*, 10(11).
539 <https://doi.org/10.3390/polym10111197>
- 540 Bordel, S., Rodríguez, E., Muñoz, R., 2019a. Genome sequence of *Methylocystis*
541 *hirsuta* CSC1, a polyhydroxyalkanoate producing methanotroph.
542 *MicrobiologyOpen*, 8(6), 1-5. <https://doi.org/10.1002/mbo3.771>
- 543 Bordel, S., Rodríguez, Y., Hakobyan, A., Rodríguez, E., Lebrero, R., Muñoz, R., 2019b.
544 Genome scale metabolic modeling reveals the metabolic potential of three Type
545 II methanotrophs of the genus *Methylocystis*. *Metab Eng*, 54, 191-199.
546 <https://doi.org/10.1016/j.ymben.2019.04.001>

547 Bordel, S., Rojas, A., Muñoz, R., 2019c. Reconstruction of a Genome Scale Metabolic
548 Model of the polyhydroxybutyrate producing methanotroph *Methylocystis*
549 *parvus* OBBP. Microb Cell Fact, 18(104). [https://doi.org/10.1186/s12934-019-](https://doi.org/10.1186/s12934-019-1154-5)
550 1154-5

551 Cal, A.J., Sikkema, W.D., Ponce, M.I., Franqui-Villanueva, D., Riiff, T.J., Orts, W.J.,
552 Pieja, A.J., Lee, C.C., 2016. Methanotrophic production of
553 polyhydroxybutyrate-co-hydroxyvalerate with high hydroxyvalerate content. Int
554 J Biol Macromol, 87, 302-307. <https://doi.org/10.1016/j.ijbiomac.2016.02.056>

555 Cantera, S., Estrada, J.M., Lebrero, R., García-Encina, P.A., Muñoz, R., 2016.
556 Comparative performance evaluation of conventional and two-phase
557 hydrophobic stirred tank reactors for methane abatement: Mass transfer and
558 biological considerations. Biotechnol Bioeng, 113(6), 1203-1212.
559 <https://doi.org/10.1002/bit.25897>

560 Cantera, S., Muñoz, R., Lebrero, R., López, J.C., Rodríguez, Y., García-Encina, P.A.,
561 2018. Technologies for the bioconversion of methane into more valuable
562 products. Curr Opin Biotechnol, 50, 128-135.
563 <https://doi.org/10.1016/j.copbio.2017.12.021>

564 Castilho, L.R., Mitchell, D.A., Freire, D.M.G., 2009. Production of
565 polyhydroxyalkanoates (PHAs) from waste materials and by-products by
566 submerged and solid-state fermentation. Bioresour Technol, 100(23), 5996-
567 6009. <https://doi.org/10.1016/j.biortech.2009.03.088>

568 Estrada, J.M., Lebrero, R., Quijano, G., Pérez, R., Figueroa-González, I., García-
569 Encina, P.A., Muñoz, R., 2014. Methane abatement in a gas-recycling
570 biotrickling filter: Evaluating innovative operational strategies to overcome

571 mass transfer limitations. Chem Eng J, 253, 385-393.
572 <https://doi.org/10.1016/j.cej.2014.05.053>

573 European Bioplastics, 2018. Bioplastics market data 2018. Global production capacities
574 of bioplastics 2018–2023. [https://www.european-bioplastics.org/wp-](https://www.european-bioplastics.org/wp-content/uploads/2016/02/Report_Bioplastics-Market-Data_2018.pdf)
575 [content/uploads/2016/02/Report_Bioplastics-Market-Data_2018.pdf](https://www.european-bioplastics.org/wp-content/uploads/2016/02/Report_Bioplastics-Market-Data_2018.pdf) (accessed:
576 15.12.2019).

577 García-Pérez, T., López, J.C., Passos, F., Lebrero, R., Revah, S., Muñoz, R., 2018.
578 Simultaneous methane abatement and PHB production by *Methylocystis hirsuta*
579 in a novel gas-recycling bubble column bioreactor. Chem Eng J, 334, 691-697.
580 <https://doi.org/10.1016/j.cej.2017.10.106>

581 Haubrichs, R., Widmann, R., 2006. Evaluation of aerated biofilter systems for microbial
582 methane oxidation of poor landfill gas. Waste Manage, 26, 408-416.
583 <https://doi.org/10.1016/j.wasman.2005.11.008>

584 IEA, 2013. AD of the organic fraction of MSW. System overview for source and central
585 separate waste. [https://www.ieabioenergy.com/wp-content/uploads/2013/09/AD-](https://www.ieabioenergy.com/wp-content/uploads/2013/09/AD-of-the-organic-fraction-of-MSW-Baxter.pdf)
586 [of-the-organic-fraction-of-MSW-Baxter.pdf](https://www.ieabioenergy.com/wp-content/uploads/2013/09/AD-of-the-organic-fraction-of-MSW-Baxter.pdf) (accessed 08.05.2020).

587 IEA, 2018. Green Gas. Facilitating a future green gas grid through the production of
588 renewable gas. IEA Bioenergy 2018. [http://task37.ieabioenergy.com/files/daten-](http://task37.ieabioenergy.com/files/daten-redaktion/download/Technical%20Brochures/green_gas_web_end.pdf)
589 [redaktion/download/Technical Brochures/green_gas_web_end.pdf](http://task37.ieabioenergy.com/files/daten-redaktion/download/Technical%20Brochures/green_gas_web_end.pdf) (accessed:
590 15.05.2020).

591 Karthikeyan, O.P., Chidambarampadmavathy, K., Nadarajan, S., Lee, P.K.H., Heimann,
592 K., 2015. Effect of CH₄/O₂ ratio on fatty acid profile and polyhydroxybutyrate
593 content in a heterotrophic–methanotrophic consortium. Chemosphere, 141, 235-
594 242. <https://doi.org/10.1016/j.chemosphere.2015.07.054>

595 Khosravi-Darani, K., Mokhtari, Z.-B., Amai, T., Tanaka, K., 2013. Microbial
596 production of poly(hydroxybutyrate) from C1 carbon sources. *Appl Microbiol*
597 *Biotechnol*, 97(4), 1407-1424. <https://doi.org/10.1007/s00253-012-4649-0>

598 Koller, M., Maršálek, L., de Sousa Dias, M.M., Braunegg, G., 2017. Producing
599 microbial polyhydroxyalkanoate (PHA) biopolyesters in a sustainable manner.
600 *New Biotechnol*, 37, 24-38. <https://doi.org/10.1016/j.nbt.2016.05.001>

601 Kraakman, N.J.R., Rocha-Rios, J., van Loosdrecht, M.C.M., 2011. Review of mass
602 transfer aspects for biological gas treatment. *Appl Microbiol Biotechnol*, 91(4):
603 873-886. <https://doi.org/10.1007/s00253-011-3365-5>

604 Lee, G.N., Na, J., 2013. Future of microbial polyesters. *Microb Cell Fact*, 12(54).
605 <https://doi.org/10.1186/1475-2859-12-54>

606 López, J., Rodríguez, Y., Pérez, V., Lebrero, R., Muñoz, R., 2019. CH₄-Based
607 Polyhydroxyalkanoate Production: A Step Further Towards a Sustainable
608 Bioeconomy, in: Kalia, V.C., (Eds), *Biotechnological Applications of*
609 *Polyhydroxyalkanoates*. Springer Singapore, Singapore, pp. 283-321.

610 López, J.C., Arnáiz, E., Merchán, L., Lebrero, R., Muñoz, R., 2018. Biogas-based
611 polyhydroxyalkanoates production by *Methylocystis hirsuta*: A step further in
612 anaerobic digestion biorefineries. *Chem Eng J*, 333, 529-536.
613 <https://doi.org/10.1016/j.cej.2017.09.185>

614 Mühlemeier, I.M., Speight, R., Strong, P.J., 2018. Biogas, Bioreactors and Bacterial
615 Methane Oxidation, in: Kalyuzhnaya, M.G., Xing, X.-H. (Eds), *Methane*
616 *Biocatalysis: Paving the Way to Sustainability*. Springer International Publishing
617 AG, pp. 213-235. https://doi.org/10.1007/978-3-319-74866-5_1

618 Muñoz, R., Meier, L., Diaz, I., Jeison, D., 2015. A review on the state-of-the-art of
619 physical/chemical and biological technologies for biogas upgrading. *Rev*

620 Environ Sci Biotechnol, 14(4), 727-759. <https://doi.org/10.1007/s11157-015->
621 9379-1

622 Myung, J., Flanagan, J.C.A., Waymouth, R.M., Criddle, C.S., 2017. Expanding the
623 range of polyhydroxyalkanoates synthesized by methanotrophic bacteria through
624 the utilization of omega-hydroxyalkanoate co-substrates. *AMB Express*, 7(1).
625 <https://doi.org/10.1186/s13568-017-0417-y>

626 Narancic, T., Verstichel, S., Reddy Chaganti, S., Morales-Gamez, L., Kenny, S.T., De
627 Wilde, B., Babu Padamati, R., O'Connor, K.E., 2018. Biodegradable Plastic
628 Blends Create New Possibilities for End-of-Life Management of Plastics but
629 They Are Not a Panacea for Plastic Pollution. *Environ Sci Technol*, 52(18),
630 10441-10452. <https://doi.org/10.1021/acs.est.8b02963>

631 Nikiema, J., Brzezinski, R., Heitz, M., 2007. Elimination of methane generated from
632 landfills by biofiltration: a review. *Rev Environ Sci Biotechnol*, 6, 261–
633 284. <http://doi.org/10.1007/s11157-006-9114-z>

634 Nyerges, G., Han, S.-K., Stein, L.Y., 2010. Effects of Ammonium and Nitrite on
635 Growth and Competitive Fitness of Cultivated Methanotrophic Bacteria. *Appl*
636 *Environ Microbiol*, 76(16), 5648. <https://doi.org/10.1128/AEM.00747-10>

637 Pérez, R., Cantera, S., Bordel, S., García-Encina, P.A., Muñoz, R., 2019. The effect of
638 temperature during culture enrichment on methanotrophic polyhydroxyalkanoate
639 production. *Int Biodeterior Biodegrad*, 140, 144-151.
640 <https://doi.org/10.1016/j.ibiod.2019.04.004>

641 Pérez, V., Lebrero, R., Muñoz, R., 2020. Comparative evaluation of biogas valorization
642 into electricity/heat and polyhydroxyalkanoates in waste treatment plants:
643 Assessing the influence of local commodity prices and current biotechnological

644 limitations ACS Sustainable Chem. Eng. <https://doi.org/10.1021/>
645 [acssuschemeng.0c01543](https://doi.org/10.1021/acssuschemeng.0c01543)

646 Pieja, A.J., Rostkowski, K.H., Criddle, C.S., 2011a. Distribution and Selection of Poly-
647 3-Hydroxybutyrate Production Capacity in Methanotrophic Proteobacteria.
648 Environ Microbiol, 62, 564-573. <https://doi.org/10.1007/s00248-011-9873-0>

649 Pieja, A.J., Sundstrom, E.R., Criddle, C.S., 2011b. Poly-3-Hydroxybutyrate Metabolism
650 in the Type II Methanotroph *Methylocystis parvus* OBBP. Appl Environ
651 Microbiol, 77(17), 6012-6019. <https://doi.org/10.1128/AEM.00509-11>

652 Pieja, A.J., Sundstrom, E.R., Criddle, C.S., 2012. Cyclic, alternating methane and
653 nitrogen limitation increases PHB production in a methanotrophic community.
654 Biores Technol 107: 385-392. <https://doi.org/10.1016/j.biortech.2011.12.044>

655 Rahnama, F., Vasheghani-Farahani, E., Yazdian, F., Shojaosadati, S.A., 2012. PHB
656 production by *Methylocystis hirsuta* from natural gas in a bubble column and a
657 vertical loop bioreactor. Biochem Eng J, 65, 51-56.
658 <https://doi.org/10.1016/j.bej.2012.03.014>.

659 Rocha-Rios, J., Bordel, S., Hernández, S., Revah, S., 2009. Methane degradation in
660 two-phase partition bioreactors. Chem Eng J, 152(1): 289-292.
661 <https://doi.org/10.1016/j.cej.2009.04.028>

662 Rocha-Rios, J., Quijano, G., Thalasso, F., Revah, S., Muñoz, R., 2011. Methane
663 biodegradation in a two-phase partition internal loop airlift reactor with gas
664 recirculation. J Chem Technol Biotechnol, 86(3), 353-360
665 <https://doi.org/10.1002/jctb.2523>

666 Rodríguez, Y., Firmino, P.I.M., Arnáiz, E., Lebrero, R., Muñoz, R., 2020. Elucidating
667 the influence of environmental factors on biogas-based polyhydroxybutyrate

668 production by *Methylocystis hirsuta* CSC1. *Sci Total Environ*, 706, 135136.
669 <https://doi.org/10.1016/j.scitotenv.2019.135136>

670 Rostkowski, K.H., Pfluger, A.R., Criddle, C.S., 2013. Stoichiometry and kinetics of the
671 PHB-producing Type II methanotrophs *Methylosinus trichosporium* OB3b and
672 *Methylocystis parvus* OBBP. *Bioresour Technol*, 132, 71-77.
673 <https://doi.org/10.1016/j.biortech.2012.12.129>

674 Sander, R., 2015. Compilation of Henry's law constants (version 4.0) for water as
675 solvent. *Atmos. Chem. Phys.*, 15(8), 4399-4981. [https://doi.org/10.5194/acp-15-](https://doi.org/10.5194/acp-15-4399-2015)
676 [4399-2015](https://doi.org/10.5194/acp-15-4399-2015)

677 Stone, K.A., Hilliard, M.V., He, Q.P., Wang, J., 2017. A mini review on bioreactor
678 configurations and gas transfer enhancements for biochemical methane
679 conversion. *Biochem Eng J*, 128, 83-92
680 <https://doi.org/10.1016/j.bej.2017.09.003>

681 Strong, J.P., Laycock, B., Mahamud, N.S., Jensen, D.P., Lant, A.P., Tyson, G., Pratt, S.,
682 2016. The Opportunity for High-Performance Biomaterials from Methane.
683 *Microorganisms*, 4(11). <https://doi.org/10.3390/microorganisms4010011>

684 Yamane, T., 1993. Yield of poly-D(-)-3-hydroxybutyrate from various carbon sources:
685 A theoretical study. *Biotechnol Bioeng* 41, 165-170.
686 <https://doi.org/10.1002/bit.260410122>

687 Zhang, T., Zhou, J., Wang, X., Zhang, Y., 2017. Coupled effects of methane
688 monooxygenase and nitrogen source on growth and poly- β -hydroxybutyrate
689 (PHB) production of *Methylosinus trichosporium* OB3b. *J Environ Sci*, 52, 49-
690 57. <https://doi.org/10.1016/j.jes.2016.03.001>

691
692

693 **Tables**

694

695 **Table 1.** Operational conditions during the CH₄ mass transfer optimization test.

Test No.	EBRT (min)	Inlet gas flow (ml min ⁻¹)	R	Virtual EBRT (min)	Inlet load (g CH ₄ m ⁻³ h ⁻¹)	Organic loading rate (g COD L ⁻¹ d ⁻¹)
1.1	30	83	0	30	202 ± 22	19.4 ± 2.1
1.2			2.5	9		
1.3			5	5		
1.4			10	3		
1.5			15	2		
1.6			30	1		
2.1	60	42	0	60	86 ± 6	8.3 ± 0.6
2.2			2.5	17		
2.3			5	10		
2.4			10	5		
2.5			15	4		
2.6			30	2		
3.1	120	21	0	120	51 ± 4	4.9 ± 0.4
3.2			2.5	34		
3.3			5	20		
3.4			10	11		
3.5			15	8		
3.6			30	4		

696

697

698

699

700 **Figure captions**

701 **Fig. 1** (a) Image and (b) Schematic representation of the experimental set-up. (1) Air
702 compressor, (2) Mixing chamber, (3) Rotameters, (4) Biogas cylinders, (5) Bubble
703 column bioreactor, (6) Condenser, (7) Liquid sampling port, (8) Gas recirculation pump,
704 (9) Thermostatic bath, (10) Gas sampling ports, (11) Magnetic stirrer, (12) Mass flow
705 controller.

706 **Fig. 2** Influence of R on the (a) CH₄-EC and on the (b) CH₄-RE at EBRTs of 30 min, 60
707 min and 120 min.

708 **Fig. 3** Influence of the virtual gas residence time on the CH₄-EC.

709 **Fig. 4** Time course of (a) CH₄-EC and PCO₂; (b) N-NO₂⁻ and N-NO₃⁻ concentration in
710 the culture broth, and N-NO₃⁻ concentration in the mineral salt medium; (c) biomass
711 concentration expressed as TSS.

712 **Fig. 5** Time course of (a) CH₄-EC and PCO₂; (b) N-NO₂⁻ and N-NO₃⁻ concentration in
713 the culture broth, and N-NO₃⁻ concentration in the mineral salt medium; (c) PHB (%)
714 and biomass concentration expressed as TSS (hexagons).

**“Biogas valorization via continuous polyhydroxybutyrate production
by *Methylocystis hirsuta* in a bubble column bioreactor”**

**Yadira Rodríguez^{a,b}, Paulo Igor Milen Firmino^{b,c}, Víctor Pérez^{a,b}, Raquel
Lebrero^{a,b}, Raúl Muñoz^{a,b,*}**

^a Department of Chemical Engineering and Environmental Technology, School of Industrial
Engineering, University of Valladolid, Dr. Mergelina s/n, 47011 Valladolid, Spain

^b Institute of Sustainable Processes, Dr. Mergelina s/n, 47011 Valladolid, Spain.

^c Department of Hydraulic and Environmental Engineering, Federal University of Ceará, Fortaleza,
Ceará, Brazil

Supplementary Material

Material and methods

S1. Electric power demand

The power demand of the internal gas recirculation and air compressors for each operational condition at the mass transfer test (2.2.2) was estimated according to the following formula (Estrada et al. 2011):

$$P \text{ (kW)} = \frac{\Delta P \cdot (Q + Q_R)}{\eta} \quad (\text{Eq.S1})$$

where ΔP represents the pressure drop (kPa), $Q + Q_R$ represent the real flow entering the column (inlet gas flow and internal recirculation flow, respectively) and η stands for the efficiency of both compressors (70%).

S2. Carbon footprint emissions

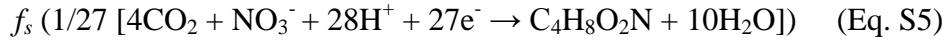
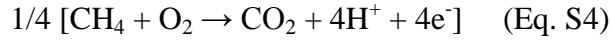
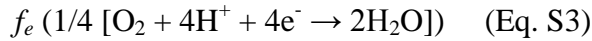
Two scenarios were evaluated to study the environmental impact in terms of CO₂ equivalents (kg CO₂ y⁻¹) of direct and indirect emissions on a 1-year basis: (1) The biogas produced in the anaerobic digester was completely vented; (2) The biogas produced in the anaerobic digester was treated in the BCB. Both scenarios were assessed at the different operating conditions of the mass transfer test.

Conversion factors for methane emission and electricity production of 25 kg CO₂ kg⁻¹ CH₄ and 0.35 kg CO₂ kWh⁻¹ were used, respectively.

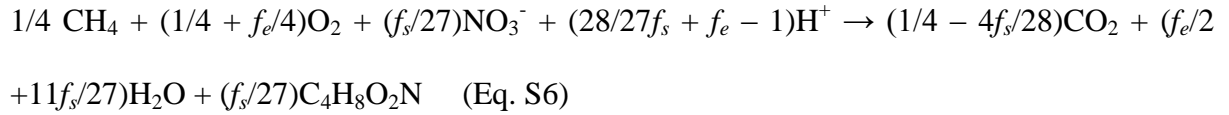
$$\text{Carbon footprint reduction (\%)} = \frac{CO_2 \text{ eq}_{(1)} - CO_2 \text{ eq}_{(2)}}{CO_2 \text{ eq}_{(1)}} \quad (\text{Eq.S2})$$

S3. Substrate partitioning coefficients (f_e and f_s) and carbon distribution

As described by Rostkowski et al. (2012), cell synthesis in methanotrophs occurs in three half reactions: (1) the reduction of the electron acceptor (O_2) into H_2O (Eq. S3); (2) the oxidation of the electron donor (CH_4) into CO_2 (Eq. S4) and (3) cell growth. The latter has been adjusted according to the formula used for cell mass ($C_4H_8O_2N$) (Khosravi-Darani et al., 2013) in the present work.

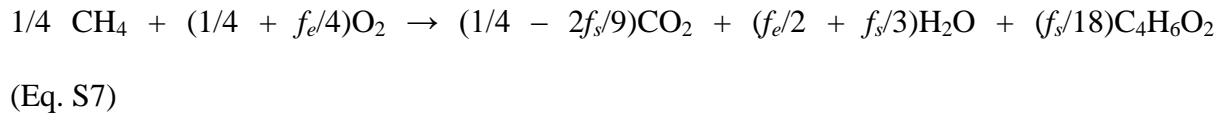


The global reaction for cell mass synthesis using NO_3^- as a nitrogen source is given by Eq. S6.



f_e and f_s represent the fraction of electrons from the substrate that are utilized for energy generation and for biomass synthesis, respectively. The sum of f_e and f_s is equal to 1.

Likewise, biopolymer ($C_4H_6O_2$) synthesis can be expressed as:



Results and discussion

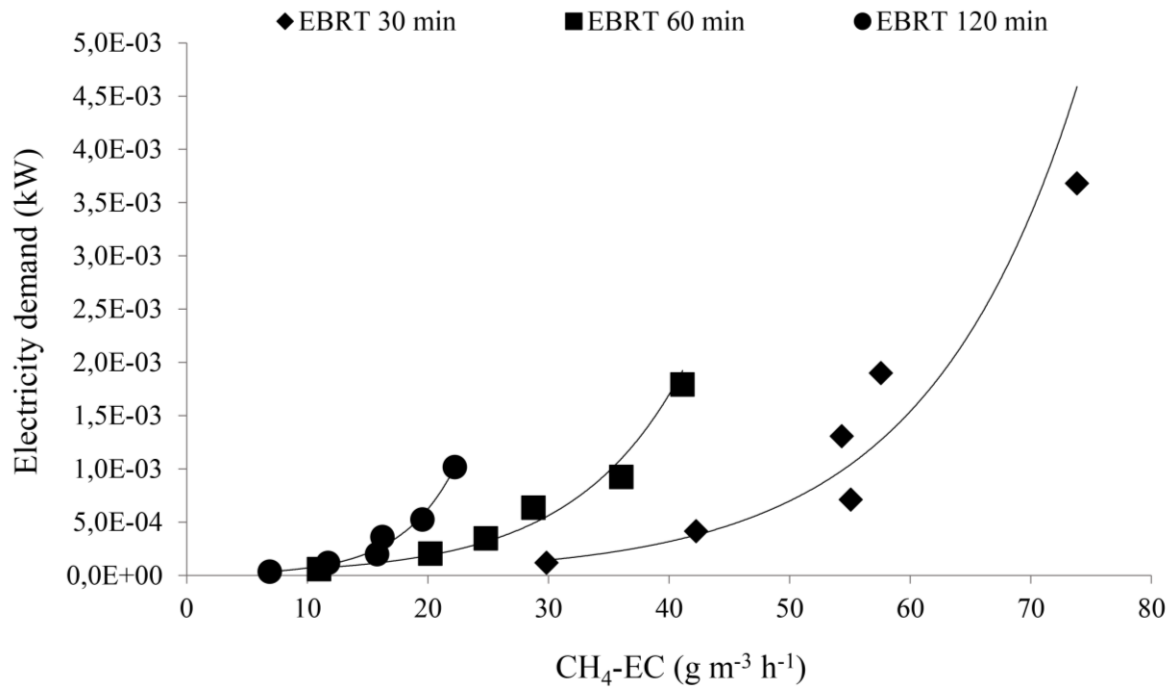


Figure S1. Power demand at different EBRTs. Each point of the curve represents the different internal recirculation rates assayed (from left to right: 0, 2.5, 5, 10, 15 and 30).

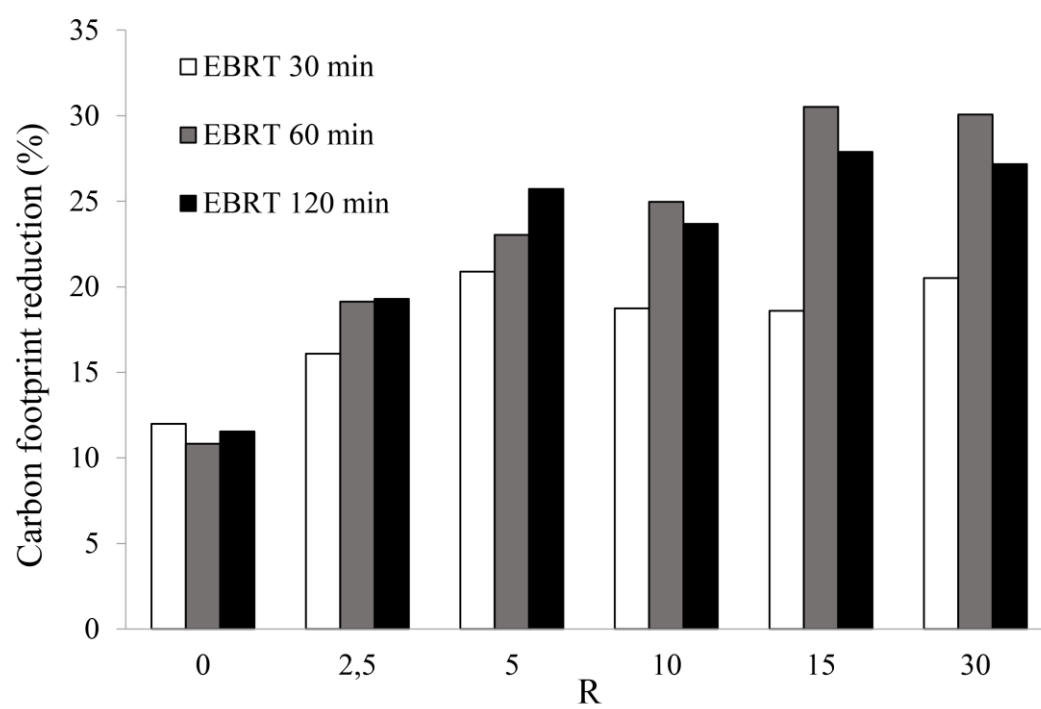


Fig. S2 Carbon footprint mitigation (%) resulting from the biological treatment at lab scale of biogas (comparison between Scenario 1 and 2).

Table S1. Electron fractions (f_e and f_s) and carbon distribution during a N feast-famine cycle (24h:24h)

Phase	f_e	f_s	Y_X (g biomass g ⁻¹ CH ₄) Y_{PHB} (g PHB g ⁻¹ CH ₄)	Carbon balances (C-g)							
				CH ₄ (in)	CO ₂ (in)	CH ₄ (out)	CO ₂ (out)	Biomass (out)	PHB (out)	TOC (out)	Balance error (%)
Growth	0.44	0.56	0.55	2.70 ± 0.11	1.07 ± 0.03	0.89 ± 0.03	2.41 ± 0.11	0.64 ± 0.06	-0.19 ± 0.02	0.04 ± 0.00	0.45
Accumulation	0.80	0.20	0.24	2.73 ± 0.07	1.05 ± 0.04	0.90 ± 0.02	2.55 ± 0.13	0.21 ± 0.01	0.32 ± 0.04	0.00 ± 0.00	5.38

REFERENCES

- Estrada, J.M., Kraakman, N.J.R., Muñoz, R., Lebrero, R., 2011. A comparative analysis of odour treatment technologies in wastewater treatment plants. *Environ Sci Technol*, 45, 1100-1106 <https://doi.org/10.1021/es103478j>
- Khosravi-Darani, K., Mokhtari, Z.-B., Amai, T., Tanaka, K., 2013. Microbial production of poly(hydroxybutyrate) from C1 carbon sources. *Appl Microbiol Biotechnol*, 97(4), 1407-1424. <https://doi.org/10.1007/s00253-012-4649-0>
- Rostkowski, K.H., Pfluger, A.R., Criddle, C.S., 2013. Stoichiometry and kinetics of the PHB-producing Type II methanotrophs *Methylosinus trichosporium* OB3b and *Methylocystis parvus* OBBP. *Bioresour Technol*, 132, 71-77. <https://doi.org/10.1016/j.biortech.2012.12.129>

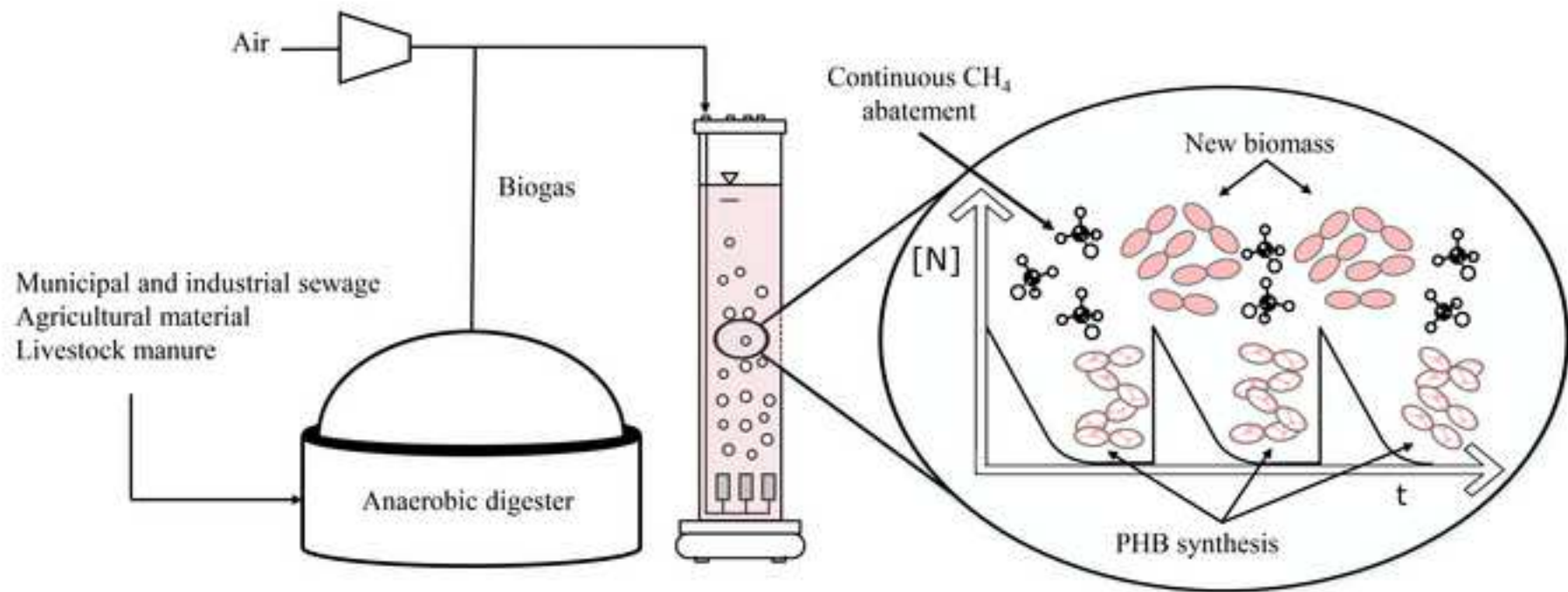


Figure 1a
[Click here to download high resolution image](#)



Figure 1b
[Click here to download high resolution image](#)

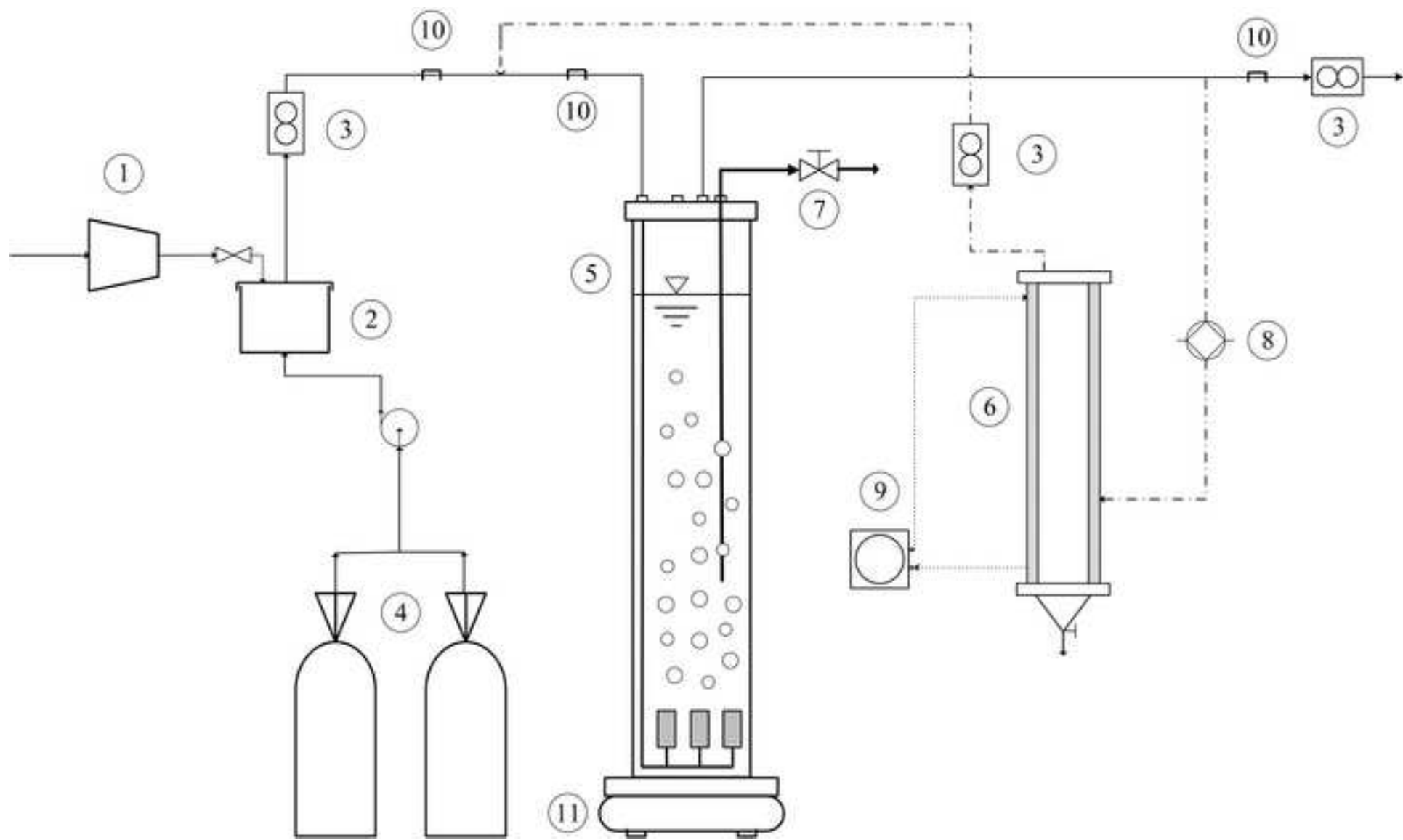


Figure 2
[Click here to download high resolution image](#)

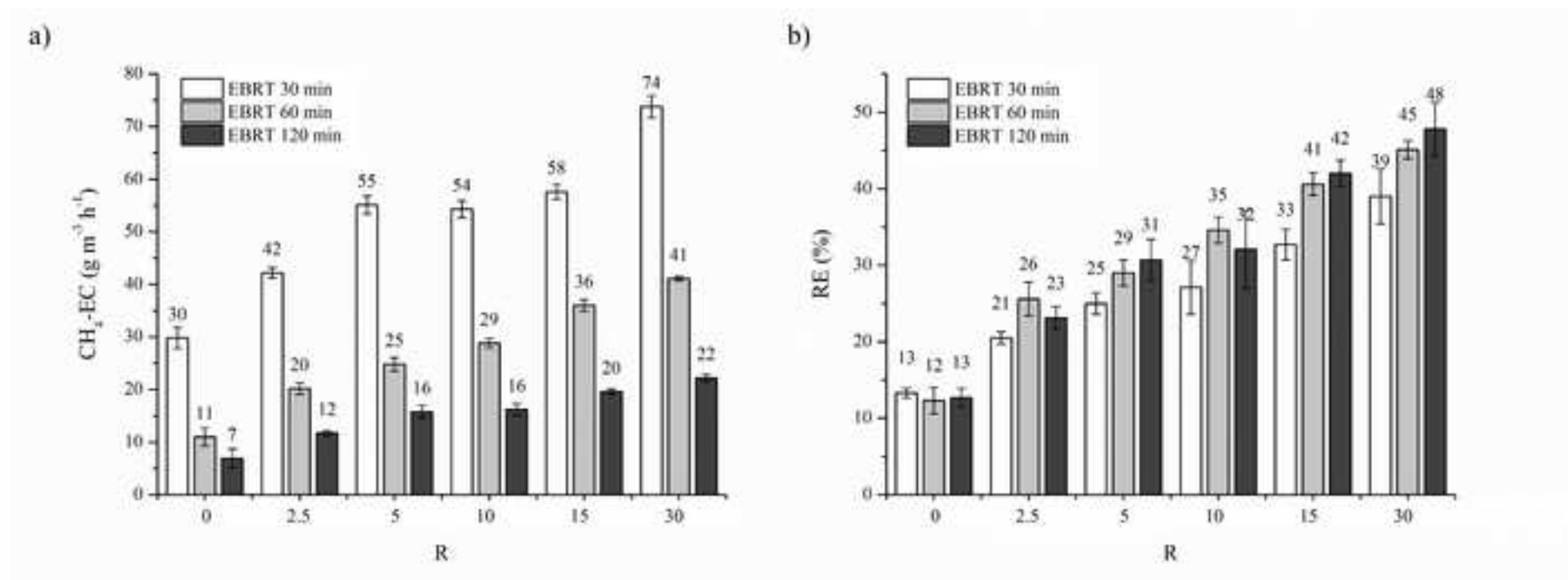


Figure 3
[Click here to download high resolution image](#)

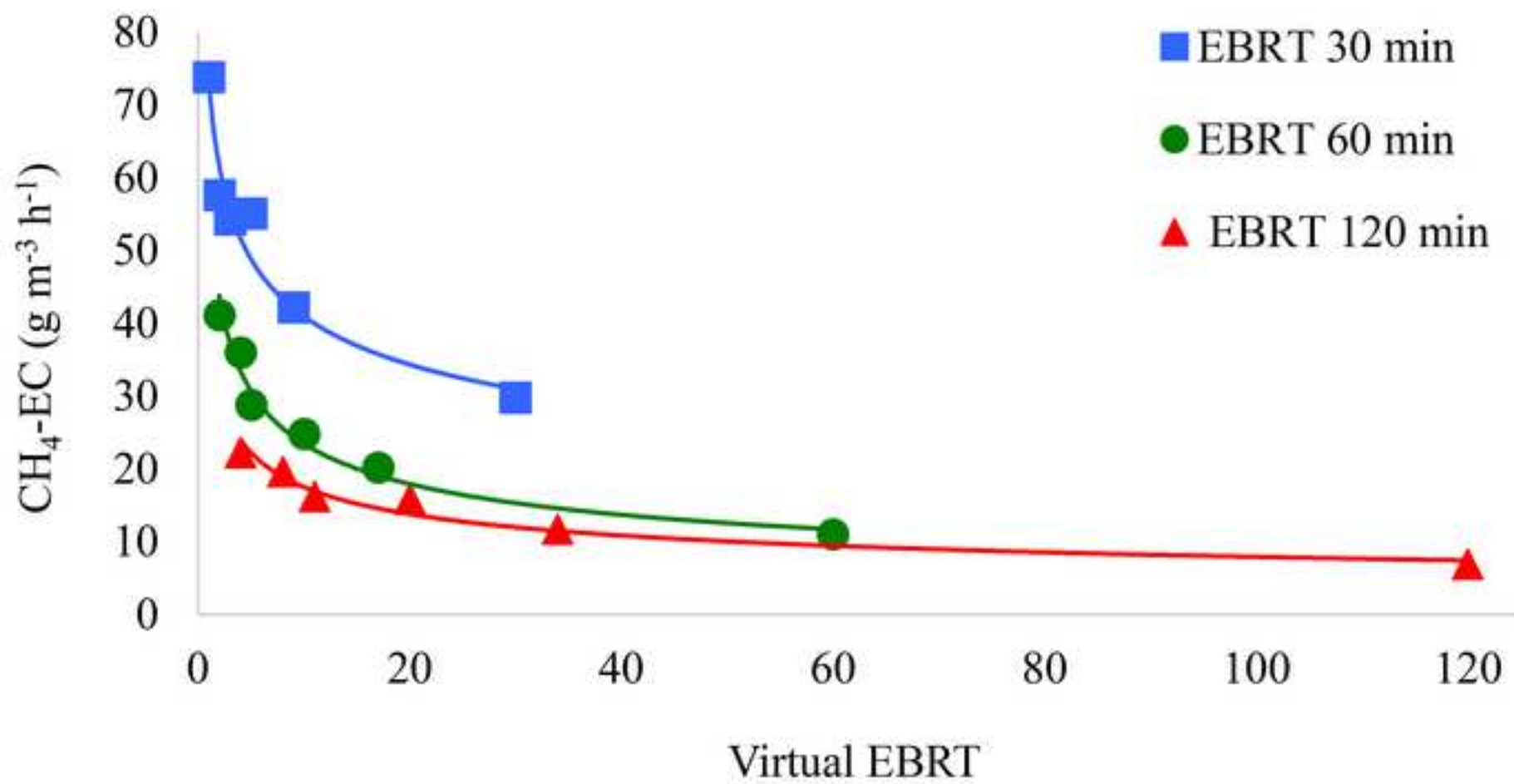


Figure 4
[Click here to download high resolution image](#)

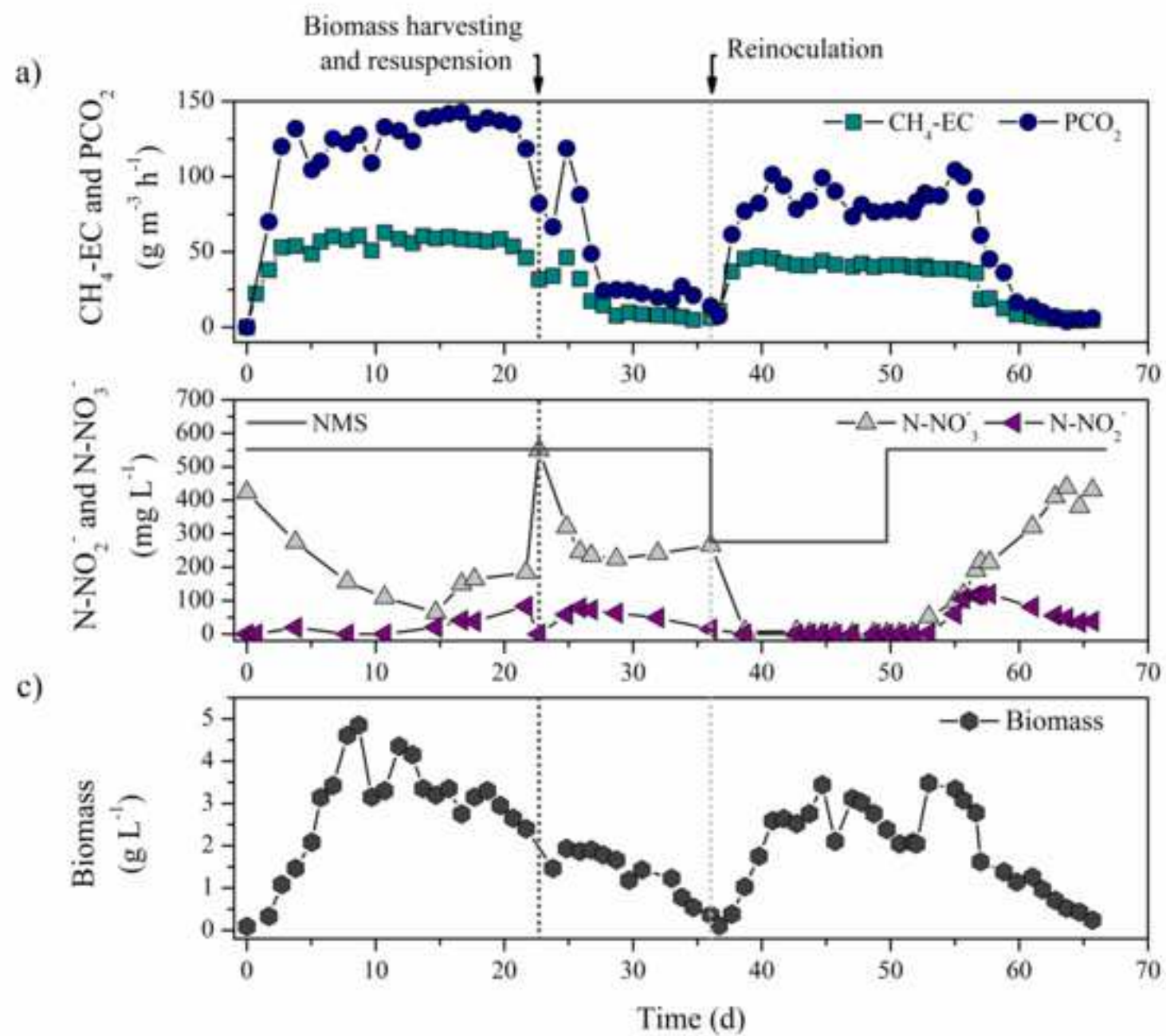


Figure 5
[Click here to download high resolution image](#)

